Nanoasperity: Structure Origin of Nacre-Inspired Nanocomposites

Shuang Xia,[†] Zuoning Wang,[†] Hong Chen,[†] Wenxin Fu,[†] Jianfeng Wang,[*,‡] Zhibo Li,[*,†,§] and Lei Jiang[†,‡]

[†]Beijing National Laboratory for Molecular Sciences (BNLMS), Institute of Chemistry, Chinese Academy of Sciences, Beijing 100190, China, [‡]Key Laboratory of Bio-inspired Smart Interfacial Science and Technology of Ministry of Education, Beijing Key Laboratory of Bio-inspired Energy Materials and Devices, School of Chemistry and Environment, BeiHang University, Beijing 100191, China, and [§]School of Polymer Science and Engineering, Qingdao University of Science and Technology, Qingdao 266042, China

ABSTRACT Natural nacre with superior mechanical property is generally attributed to the layered "brick-and-mortar" nanostructure. However, the role of nanograins on the hard aragonite platelets, which is so-called nanoasperity, is rarely addressed. Herein, we prepared silica platelets with aragonite-like nanoasperities via biomineralization strategy and investigated the effects of nanoasperity on the mechanical properties of resulting layered nanocomposites composed of roughened silica platelets and poly(vinyl alcohol). The tensile deformation behavior of the nanocomposites demonstrates that nanograins on silica platelets are responsive for strain hardening, improved strength, and toughness. The structure origin is attributed to the nanoasperity-controlled platelet sliding.

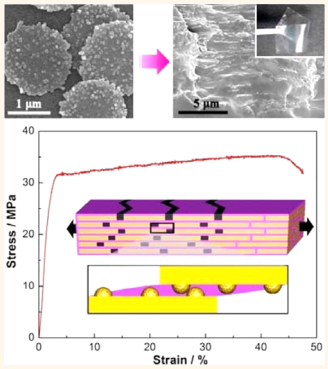

KEYWORDS: biomineralization · bioinspired materials · hierarchical structure · nacre · nanoasperities

Natural nacre develops a hierarchical microstructure through a biomineralized process to optimize its mechanical properties.[1,2] The typical microstructure of nacre embraces two levels of hierarchy.[3,4] In the first level, aragonite platelets are decorated with nanograins on the surface (Figure 1a). In the second level, nanostructured aragonite platelets and biopolymers are alternately stacked into "brick-and-mortar" layered microstructure (Figure 1b), which is demonstrated to play a key role in the integration of excellent toughness and strength.[5] The highly oriented layered structure helps to carry load in the direction parallel to the lamellae, while the nanoasperities could modulate the sliding of aragonite platelets via contact friction and generate high stress to attain inelastic strain.[6,7]

In nacre-inspired hybrid materials, great attempts have been made to mimic the second level of hierarchy in nacre and built layered composites through a range of assembly techniques based on inorganic micro/nanoplatelets.[8] The employed micro/nanoplatelets include clays,[9−16] Al_2O_3,[17] layered double hydroxides (LDH),[18,19] graphene oxide,[20−24] and other artificial platelets.[25,26] Although the mimic protocol is rather simple, the first level of hierarchy, such as the surface roughness of the "bricks", is hard to accomplish.[27] Since most reported micro/nanoplatelets feature a smooth surface, which is in contrast to the rough aragonite platelets in natural nacre, it is highly desirable to replicate the hierarchical microstructure of nacre instead of simple layered structure.[28,29]

To construct nacre-like hierarchical microstructure, the key challenge is to create synthetic "brick" with nanoasperities. It is well-known that polypeptide-templated biomineralization is a highly controllable route to obtain well-defined organic−inorganic nanoobjects under benign reaction conditions.[30,31] We recently demonstrated that a double hydrophilic poly(ethylene glycol)-*b*-poly-L-lysine (PEG−PLL) could direct formation of silica platelets, which can be redispersed in polar solvents.[32] Moreover, both rough and smooth silica platelets with controllable size and morphology can be readily prepared in large quantity. To fabricate layered nanocomposites, the rough or smooth silica platelets and poly(vinyl alcohol) (PVA) are alternately stacked into layered structure through

* Address correspondence to zbli@iccas.ac.cn, wangjianfeng@buaa.edu.cn.

Received for review January 8, 2015 and accepted January 27, 2015.

Published online January 27, 2015
10.1021/acsnano.5b00119

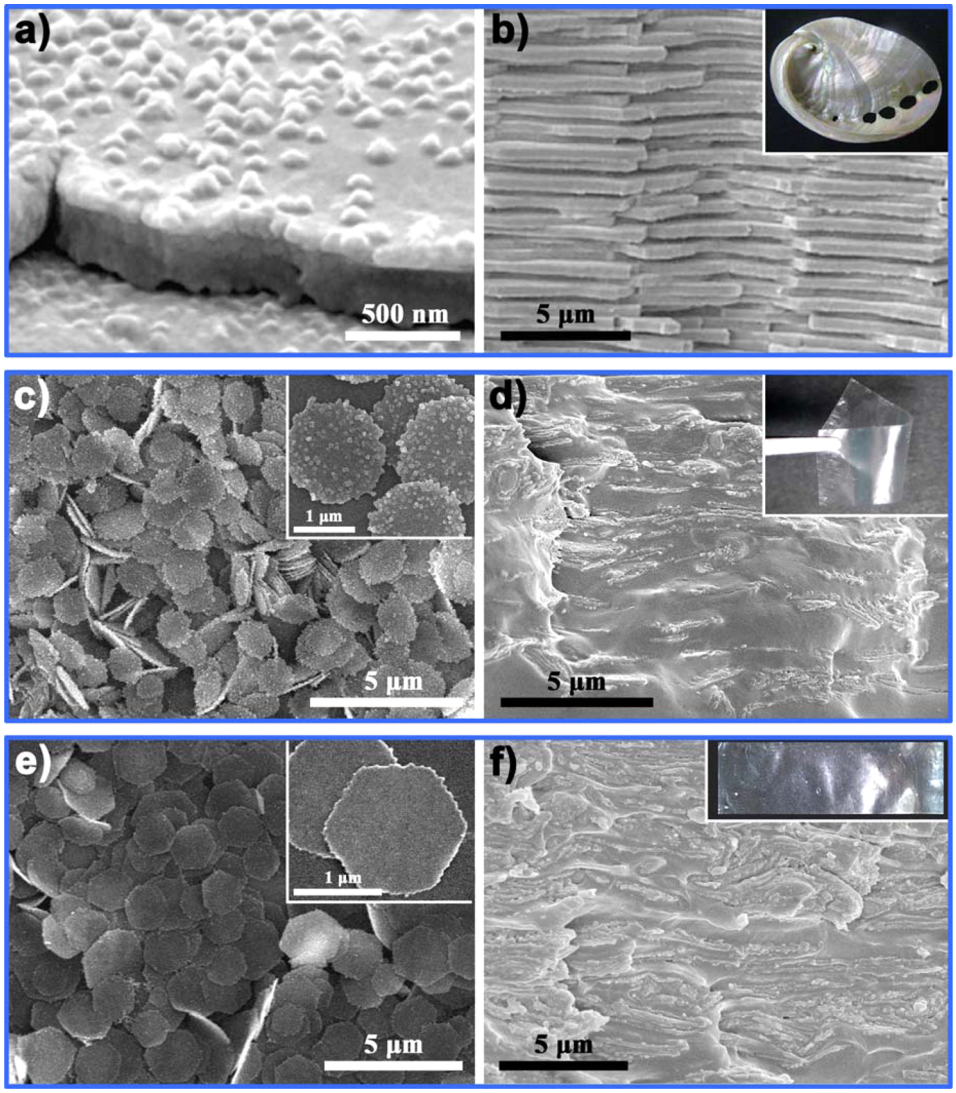

Figure 1. Comparison between layered films fabricated with rough/flat platelets and natural nacre stacked with aragonite platelets. (a) Nanograins on the platelets of red abalone.[35] (b) SEM of fracture surface of inner nacreous layer in red abalone shell.[36] Inset: digital photo of inner nacreous layer of the nacre. (c) SEM of rough platelets in high (inset) and low magnification. (d) Fracture surface of layered films fabricated with rough platelets after quenching by liquid nitrogen and the photo of fabricated films (inset). (e) Platelets with flat surface shown in high (inset) and low magnification. (f) Fracture surface of layered films fabricated with flat platelets after quenching and the corresponding fabricated films (inset).

dip-coating strategy. The correlation between the hierarchical structure and tensile deformation behaviors is investigated. Different from smooth platelets, rough platelets induce strain hardening, further leading to improved strength and toughness. Cyclic loading−unloading behaviors then verify the nanoasperity-controlled deformation through platelet contact friction.

RESULTS AND DISCUSSION

The surface roughened SiO_2 platelets used in present study were synthesized employing PEG_{114}-PLL_{68} copolymer as template (^{1}H NMR of PEG_{114}-PLL_{68}; see Supporting Information, Figure S1). The diblock copolymer directed the precipitation of SiO_2 platelets through electrostatic interactions and hydrogen bonding between PLL block and the negatively charged silicic acid precursor,[33] while the PEG block was responsive for the stable dispersion of nanoparticles in polar solvents. The surface characteristic of platelets mainly depended on the proportion of copolymer and silicic acid (see Methods for details). Given the excess silicic acid condition, plenty of nanograins were attached to the surface of platelets to offer rough platelets (RP) with uniform size (Figure 1c). RP is essentially a closer mimic to aragonite platelets found in natural nacre as compared to those reported examples.[34] The typical lateral dimension and thickness of RP were about 1.4 μm and 13 nm, respectively, while the height of nanograins is 5−7 nm with a distribution in the order of 100−300 nm (Figure S2a). We further found that nanograins were bound firmly to the surface of platelets since they can maintain their integrity after ultrasound or stress treatment (Figures S3 and S4). In order

to investigate the effect of nanoasperities on the overall mechanical response, we also prepared flat platelets (FP) with smooth surface using the same method except that less silicic acid precursors were applied in contrast to RP (Figure 1e). Sizes of the FP were deliberately chosen, and the lateral dimension and thickness were close to RP (1.6 μm $\times$ 12 nm, Figure S2b). Two as-prepared platelets are both positively charged in water and could be easily redispersed in polar solvents (Figure S5), conducive to fabrication of uniform composite films.

The layered hybrid films were fabricated based on sequential adsorption of platelets (ethanol suspension) and PVA (water solution). The adsorption of the two materials was favored through hydrogen bonding between $-$OH of PVA and Si$-$O$-$Si on the platelet surface (Figure S6), and SEM verified the dense coverage of the platelets on the PVA layer (Figure S7). Sequential repetition led to multilayered hybrid films (RP/P and FP/P, insets of Figure 1d,f). We tuned the platelet loading through altering the weight concentrations of PVA solution (0.5, 1, and 2 wt %). Pure PVA films were also prepared as control samples *via* solution casting. Thermogravimetric analysis shows that RP/P and FP/P fabricated with the same PVA concentration were composed of nearly the same platelet weight fractions (RP/P-16, 25, 40 and FP/P-15, 24, 41, numbers in sequence represent platelets fraction in wt %, Figure S8). The cross-sectional SEM after quenching by liquid nitrogen reveals a good alignment of both RPs and FPs (Figure 1d,f).

Figure 2a plots the stress$-$strain curves of both RP/P and FP/P hybrid composites with different compositions. The pure PVA films show a large tensile strain of 65%, but low Young's modulus of 600 MPa and tensile strength of 14 MPa (Table S1). Compared with pure PVA, the hybrid composite film with 40 wt % RP displays 4.5 times higher Young's modulus and nearly 4-fold higher tensile strength. Other mechanical properties are also impressive, especially tensile toughness (Table S1). Most remarkably, RP/P with high platelet contents tends to display continuous strain hardening and develops exceptional tensile toughness under deformation (Figure 2a). For FP/P, the Young's modulus and the ultimate strain are comparable to RP/P, while featuring a lower strength and tensile roughness particularly at higher platelet contents (Table S1). In stark contrast to strain hardening of RP/P, FP/P shows significant softening after yielding and holds the response up to failure. The comparison of tensile test results indicates that nanoasperity is an essential ingredient in strain hardening and plays a crucial role in strength and toughness.

To elucidate the mechanisms of the strain hardening and impressive toughness of RP/P, surface and fracture morphology of RP/P tensile specimens with high platelet contents were examined. A great number of narrow

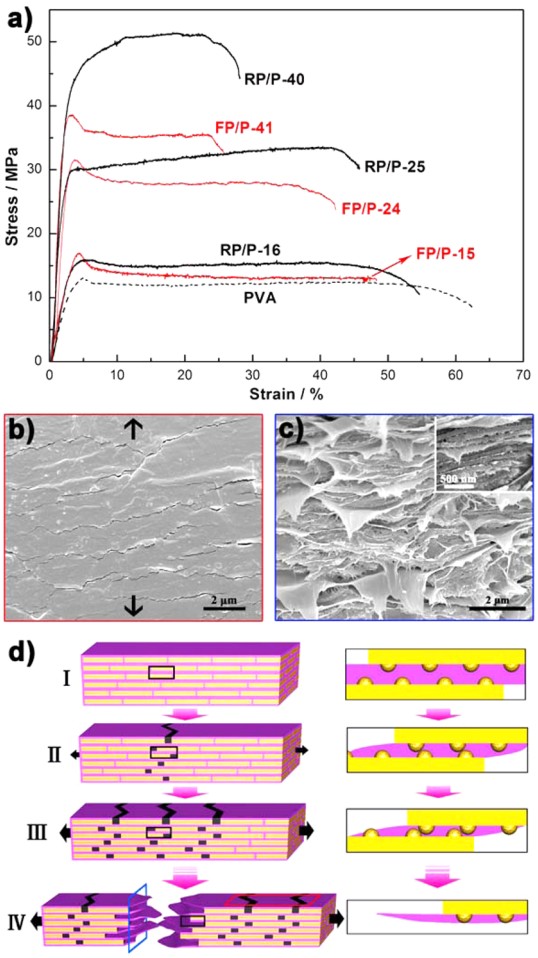

Figure 2. Mechanical tensile properties of the layered films and proposed deformation mechanisms. (a) The tensile stress$-$strain curves of RP/P, FP/P, and pure PVA. (b) SEM of a tensile specimen of RP/P (top surface) and microcracks can be found in large areas. Arrows indicate the direction of tensile stress. (c) SEM of fracture surface of RP/P. Inset shows the profile morphology of contacted RPs after stretching. (d) Proposed deformation processes: initial configuration (I), deformation (II, III), and failure processes (IV). The regions in IV labeled by red and blue joint lines correspond to the SEM morphologies of panels b and c, respectively.

microcracks was observed on the surface of RP/P tensile specimen (Figure 2b), possibly derived from the extensive sliding of interior platelets. On the basis of the irregular morphology of the fracture surface (Figure 2c and inset), it is considered that the ductile rupture occur under platelet pull-out mode rather than platelet fracture.[17] According to the information on mechanical response and developed morphologies under stress loading, we have proposed the deformation processes of present nacre-inspired nanocomposites, as schematically shown in Figure 2d. Under loading in tension along the platelets plane, rough platelets start to slide at one point accompanied by the shear deformation of PVA interlayer when the yield stress is reached. Accordingly, the interfacial gap between adjacent platelets decreases. After sliding to a certain distance, the nanograins on RP surface start

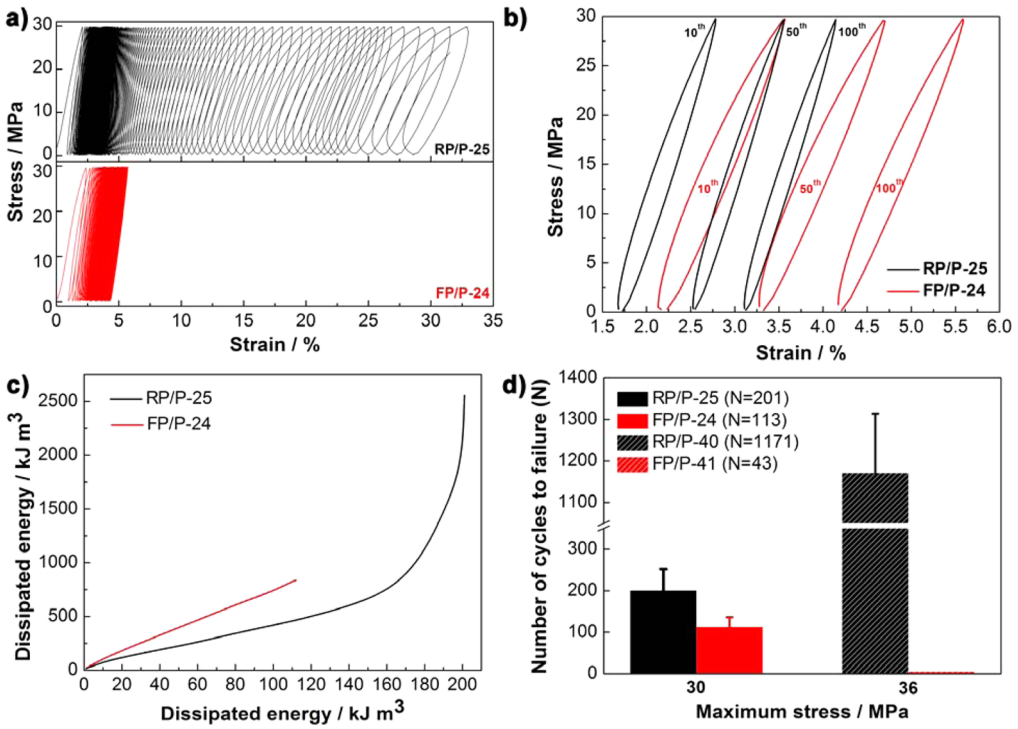

Figure 3. Cyclic loading−unloading behaviors of RP/P and FP/P. (a) Cyclic loading−unloading curves of RP/P-25 (up) and FP/P-24 (down) at maximum loading stress of 30 MPa. (b) Corresponding loading−unloading curves of RP/P-25 and FP/P-24 at 10th, 50th, and 100th cycle. (c) The accumulated areas of sequential single cycle in terms of dissipated energy of RP/P-25 and FP/P-24. (d) Maximum tensile stresses versus the number of cycles to failure of RP/P-25, 40 and FP/P-24, 41.

to contact and interact (Figure 2d, I to II), which results in mechanically interlocking of the local platelets and generating higher stress, *i.e.* strain hardening (Figure 2a). The increased stress triggers new sliding sites of adjacent platelets during the process of climbing obstacles (Figure 2d, III). The sliding-contact-triggering-climb process proceeds repeatedly until all potential sliding sites are exhausted. Finally, platelets pull out leaving PVA under high shear stress, and the specimen fails after fracturing of PVA interlayers (Figure 2b, schematic shown in IV of Figure 2d). Platelet sliding occurs at a large volume, resulting in the development of many narrow microcracks on the top surface (Figure 2c, schematic shown in IV of Figure 2d). Energy dissipation also pervades through a relatively large volume, rather than only at the fracture surface, leading to large tensile toughness. As for FP/P, because of the absence of nanoasperities, platelets slide in a relatively uncontrollable way (Scheme S1). Centralized wide microcracks can be randomly observed on the fracture surface of tensile specimen FP/P (Figure S9), and significant softening and lower tensile roughness are measured (Figure 2a).

To further confirm the role of nanoasperities in the deformation process, cyclic loading−unloading test is performed in tensile mode.[37−39] The samples were loaded to maximum applied stresses close to yield strength at 10 MPa/min and then unloaded to 0 at 60 MPa/min (see Methods for details). The cyclic stress−strain curves for RP/P-25 and FP/P-24 are shown in Figure 3a. It can be found that RP/P-25 has higher strain at break and cyclic number than those of FP/P-25. The representative single cycles were extracted from the cyclic stress−strain curves (Figure 3b). Compared with FP/P-24, RP/P-25 shows an obviously smaller strain at the same number of cycles, which indicates that the nanoasperities on rough platelet surface indeed play a direct role in retarding the sliding of platelets, as proposed in Figure 2d. Another obvious distinction is that the area enclosed by loading and unloading curves of RP/P-25 is smaller than that of FP/P-24. The area represents the energy dissipated per unit volume of materials through plastic deformation of PVA, which reflects the permanent damage of microstructure. The area of every cycle was integrated and then sequentially accumulated. Thus, the dependence of the accumulated energy on the number of cycles was obtained (Figure 3c). RP/P-25 shows slower energy dissipation rate than FP/P-24, and the total energy dissipation for RP/P-25 before fracture is about three times higher than FP/P-24. These results mean that nanoasperity-controlled sliding decreases the energy dissipation rate and improves the gross energy dissipation, which leads to improved cyclic life and corresponds to fatigue-resistance behaviors (Figure 3d). The mean cyclic life of RP/P-25 is 180% higher than that of FP/P-24 at the maximum stress of 30 MPa. Such variation trend is also reflected in the comparison of RP/P-40 with FP/P-41 (Figure S10). Surprisingly, the mean cycle life of RP/P-40 is about 27 times higher

than FP/P-41 at 36 MPa. The results of cyclic tests further confirm that nanoasperities play a critical role in controlling the sliding of platelets and avoiding premature failure of materials, as proposed in Figure 2d.

CONCLUSION

In conclusion, we have fabricated hierarchical composites in a close mimic of natural nacre employing artificial platelets with unique nanoasperities. These platelets were prepared *via* biomineralization strategy with great control over their surface roughness and dimensions. The tensile deformation behavior of present nanocomposites suggested that incorporation of nanoasperities could achieve a remarkable mechanical response of strain hardening, as well as enhanced strength and tensile roughness. The cyclic tests further provided proof of the nanoasperity-controlled sliding. These results provided an insight into the effect of nanoasperities on tensile deformation behaviors and further confirmed the significant role of nanoasperities on natural nacre. Our model materials could offer a new concept to optimize the mechanical properties of bioinspired layered composites.

METHODS

Preparation of Rough Platelets and Flat Platelets. We prepared two platelets through the method of biomineralization using PEG_{114}-*b*-PLL_{68} diblock copolymers as template. Rough platelets (RPs) were prepared under excess silicic acid conditions. Typically, 100 μL of PEG_{114}-*b*-PLL_{68} solution (10−15 mg/mL) was dispersed in 20 μL of sodium phosphate buffer (pH 7.5, 0.1 M) for about 4 min. Then a freshly prepared solution of silicic acid (60 μL TMOS mixed with 15 μL, 1 M HCl) was added to the above mixture. The products were then isolated via centrifuge and dried in vacuum oven. To obtain flat platelets, higher content of buffer (80 μL) and lower TMOS content (15 μL), which hydrolyzed in 85 μL HCl (1 M), were used.

Preparation of RP/P and FP/P Layered Films. Dip-coating was used to fabricate layered films through the hydrogen-bonding interactions between PVA (M_w: 9000−10000, Sigma-Aldrich) and platelets. In a typical procedure, platelets were first dispersed in ethanol by ultrasound to form 2 mg/mL dispersion, and then a cleaned silicon wafer was immersed in the dispersion for 5 min. After being rinsed by deionized water and completely dried in air, the silicon wafer was immersed in PVA solution (0.5, 1, or 2 wt %) for another 5 min, and again rinsed by deionized water and dried on a heating stage. This procedure gave a bilayer of platelets/PVA. The cycle could be repeated to obtain the desired number of bilayers. Free-standing hierarchical films with desired thicknesses were peeled from the silicon wafer. The obtained films were further dried on the heating stage at 65 °C for 1 h and then dried in a desiccator for 1 day prior to mechanical tests.

Characterization. The SEM images were obtained with a field emission scanning electron microscope (S-4800, Hitachi and JEOL-6700) at an acceleration voltage of 5 kV. The mechanical properties of the hierarchical films were carried out on an Instron 3365 universal mechanical testing machine at room temperature (23 ± 2 °C, 55% relative humidity) with a crosshead speed of 2 mm/min, and at least 5 replicates were tested for each sample to obtain tensile properties. The cyclic loading and unloading tests were carried out on dynamic mechanical analysis (DMA, TA DMA Q800 instrument). The sample tested on various maximum stresses always referred to a sample that had not been previously deformed. The test temperature was 25 ± 1 °C, with the use of an air-compressed jet to maintain a constant, controlled temperature. The specimens were clamped to two metal clamps, resulting in specimens measuring (5 ± 0.2) × (5 ± 0.2) × (0.02 ± 0.005) mm^3 (length × wide × thickness). The program was as follows: (1) ramp stress 10 to 30 MPa/min; (2) ramp stress 60 to 0 MPa/min; (3) repeat segment 1 for 10 000 times. Atomic force microscopy (AFM, Multimode 8, Digital Instruments) was performed in the ScanAsyst mode in an ambient atmosphere. Zeta potential of the platelets was measured in water dispersion using a Zetasizer (Nano Series, Malvern Instruments, U.K.) at 25 °C. X-ray photoelectron spectroscopy (XPS) data were obtained from an ESCALab220i-XL electron spectrometer from VG Scientific using 300 W AlKα radiation. The platelet amounts were assessed by thermogravimetry analysis (TGA, Pyris 1 TGA from PerkinElmer). The samples were heated up to 800 °C at a heating rate of 10 °C/min under air atmosphere.

Conflict of Interest: The authors declare no competing financial interest.

Acknowledgment. This work was supported by the National Basic Research Program of Ministry of Science and Technology of China (2012CB933201) and National Natural Science Foundation of China (51225306 and 51403008).

Supporting Information Available: ^{1}H NMR, AFM images, SEM images, zeta potential, XPS curves, TGA results, scheme of FP/P deformation processes under loading, and table for comparison of mechanical properties. This material is available free of charge *via* the Internet at http://pubs.acs.org.

REFERENCES AND NOTES

1. Meyers, M. A.; Chen, P. Y.; Lin, A. Y. M.; Seki, Y. Biological Materials: Structure and Mechanical Properties. *Prog. Mater. Sci.* **2008**, *53*, 1–206.
2. Espinosa, H. D.; Rim, J. E.; Barthelat, F.; Buehler, M. J. Merger of Structure and Material in Nacre and Bone - Perspectives on De Novo Biomimetic Materials. *Prog. Mater. Sci.* **2009**, *54*, 1059–1100.
3. Li, X.; Chang, W.-C.; Chao, Y. J.; Wang, R.; Chang, M. Nanoscale Structural and Mechanical Characterization of a Natural Nanocomposite Material: The Shell of Red Abalone. *Nano Lett.* **2004**, *4*, 613–617.
4. Li, X.; Xu, Z.-H.; Wang, R. *In Situ* Observation of Nanograin Rotation and Deformation in Nacre. *Nano Lett.* **2006**, *6*, 2301–2304.
5. Yao, H.-B.; Ge, J.; Mao, L.-B.; Yan, Y.-X.; Yu, S.-H. 25th Anniversary Article: Artificial Carbonate Nanocrystals and Layered Structural Nanocomposites Inspired by Nacre: Synthesis, Fabrication and Applications. *Adv. Mater.* **2014**, *26*, 163–188.
6. Evans, A. G.; Suo, Z.; Wang, R. Z.; Aksay, I. A.; He, M. Y.; Hutchinson, J. W. Model for the Robust Mechanical Behavior of Nacre. *J. Mater. Res.* **2001**, *16*, 2475–2484.
7. Wang, R. Z.; Suo, Z.; Evans, A. G.; Yao, N.; Aksay, I. A. Deformation Mechanisms in Nacre. *J. Mater. Res.* **2001**, *16*, 2485–2493.
8. Cheng, Q.; Jiang, L.; Tang, Z. Bioinspired Layered Materials with Superior Mechanical Performance. *Acc. Chem. Res.* **2014**, *47*, 1256–1266.
9. Tang, Z. Y.; Kotov, N. A.; Magonov, S.; Ozturk, B. Nanostructured Artificial Nacre. *Nat. Mater.* **2003**, *2*, 413–U8.
10. Podsiadlo, P.; Tang, Z.; Shim, B. S.; Kotov, N. A. Counterintuitive Effect of Molecular Strength and Role of Molecular Rigidity on Mechanical Properties of Layer-by-Layer Assembled Nanocomposites. *Nano Lett.* **2007**, *7*, 1224–1231.

11. Podsiadlo, P.; Liu, Z.; Paterson, D.; Messersmith, P. B.; Kotov, N. A. Fusion of Seashell Nacre and Marine Bioadhesive Analogs: High-Strength Nanocomposite by Layer-by-Layer Assembly of Clay and L-3,4-Dihydroxyphenylalanine Polymer. *Adv. Mater.* **2007**, *19*, 949–955.
12. Podsiadlo, P.; Kaushik, A. K.; Arruda, E. M.; Waas, A. M.; Shim, B. S.; Xu, J.; Nandivada, H.; Pumplin, B. G.; Lahann, J.; Ramamoorthy, A.; *et al.* Ultrastrong and Stiff Layered Polymer Nanocomposites. *Science* **2007**, *318*, 80–83.
13. Priolo, M. A.; Gamboa, D.; Holder, K. M.; Grunlan, J. C. Super Gas Barrier of Transparent Polymer–Clay Multilayer Ultrathin Films. *Nano Lett.* **2010**, *10*, 4970–4974.
14. Walther, A.; Bjurhager, I.; Malho, J.-M.; Ruokolainen, J.; Berglund, L.; Ikkala, O. Supramolecular Control of Stiffness and Strength in Lightweight High-Performance Nacre-Mimetic Paper with Fire-Shielding Properties. *Angew. Chem., Int. Ed.* **2010**, *49*, 6448–6453.
15. Yao, H.-B.; Mao, L.-B.; Yan, Y.-X.; Cong, H.-P.; Lei, X.; Yu, S.-H. Gold Nanoparticle Functionalized Artificial Nacre: Facile *in Situ* Growth of Nanoparticles on Montmorillonite Nanosheets, Self-Assembly, and Their Multiple Properties. *ACS Nano* **2012**, *6*, 8250–8260.
16. Wang, J. F.; Cheng, Q. F.; Lin, L.; Jiang, L. Synergistic Toughening of Bioinspired Poly(vinyl alcohol)-Clay-Nanofibrillar Cellulose Artificial Nacre. *ACS Nano* **2014**, *8*, 2739–2745.
17. Bonderer, L. J.; Studart, A. R.; Gauckler, L. J. Bioinspired Design and Assembly of Platelet Reinforced Polymer Films. *Science* **2008**, *319*, 1069–1073.
18. Yao, H.-B.; Fang, H.-Y.; Tan, Z.-H.; Wu, L.-H.; Yu, S.-H. Biologically Inspired, Strong, Transparent, and Functional Layered Organic–Inorganic Hybrid Films. *Angew. Chem., Int. Ed.* **2010**, *49*, 2140–2145.
19. Han, J.; Dou, Y.; Yan, D.; Ma, J.; Wei, M.; Evans, D. G.; Duan, X. Biomimetic Design and Assembly of Organic-Inorganic Composite Films with Simultaneously Enhanced Strength and Toughness. *Chem. Commun.* **2011**, *47*, 5274–5276.
20. Xu, Y.; Wu, Q.; Sun, Y.; Bai, H.; Shi, G. Three-Dimensional Self-Assembly of Graphene Oxide and DNA into Multifunctional Hydrogels. *ACS Nano* **2010**, *4*, 7358–7362.
21. Li, Y.-Q.; Yu, T.; Yang, T.-Y.; Zheng, L.-X.; Liao, K. Bioinspired Nacre-Like Composite Films Based on Graphene with Superior Mechanical, Electrical, and Biocompatible Properties. *Adv. Mater.* **2012**, *24*, 3426–3431.
22. Cheng, Q.; Wu, M.; Li, M.; Jiang, L.; Tang, Z. Ultratough Artificial Nacre Based on Conjugated Cross-Linked Graphene Oxide. *Angew. Chem., Int. Ed.* **2013**, *125*, 3863–3863.
23. Hu, K.; Gupta, M. K.; Kulkarni, D. D.; Tsukruk, V. V. Ultra-Robust Graphene Oxide-Silk Fibroin Nanocomposite Membranes. *Adv. Mater.* **2013**, *25*, 2301–2307.
24. Zhang, M.; Huang, L.; Chen, J.; Li, C.; Shi, G. Ultratough, Ultrastrong, and Highly Conductive Graphene Films with Arbitrary Sizes. *Adv. Mater.* **2014**, *26*, 7588–7592.
25. Burghard, Z.; Zini, L.; Srot, V.; Bellina, P.; Aken, P. A. v.; Bill, J. Toughening through Nature-Adapted Nanoscale Design. *Nano Lett.* **2009**, *9*, 4103–4108.
26. Tritschler, U.; Zlotnikov, I.; Zaslansky, P.; Fratzl, P.; Schlaad, H.; Cölfen, H. Hierarchically Structured Vanadium Pentoxide–Polymer Hybrid Materials. *ACS Nano* **2014**, *8*, 5089–5104.
27. Wegst, U. G. K.; Bai, H.; Saiz, E.; Tomsia, A. P.; Ritchie, R. O. Bio-Inspired Structural Materials. *Nat. Mater.* **2015**, *14*, 23–36.
28. Munch, E.; Launey, M. E.; Alsem, D. H.; Saiz, E.; Tomsia, A. P.; Ritchie, R. O. Tough, Bioinspired Hybrid Materials. *Science* **2008**, *322*, 1516–1520.
29. Naglieri, V.; Bale, H. A.; Gludovatz, B.; Tomsia, A. P.; Ritchie, R. O. On the Development of Ice-Templated Silicon Carbide Scaffolds for Nature-Inspired Structural Materials. *Acta Mater.* **2013**, *61*, 6948–6957.
30. Cha, J. N.; Stucky, G. D.; Morse, D. E.; Deming, T. J. Biomimetic Synthesis of Ordered Silica Structures Mediated by Block Copolypeptides. *Nature* **2000**, *403*, 289–292.
31. Chen, C.-L.; Rosi, N. L. Peptide-Based Methods for the Preparation of Nanostructured Inorganic Materials. *Angew. Chem., Int. Ed.* **2010**, *49*, 1924–1942.
32. Chen, H.; Xia, L.; Fu, W.; Yang, Z.; Li, Z. One-Step Synthesis of Water Dispersible Silica Nanoplates. *Chem. Commun.* **2013**, *49*, 1300–1302.
33. Coradin, T.; Durupthy, O.; Livage, J. Interactions of Amino-Containing Peptides with Sodium Silicate and Colloidal Silica: A Biomimetic Approach of Silicification. *Langmuir* **2002**, *18*, 2331–2336.
34. Lin, T.-H.; Huang, W.-H.; Jun, I.-K.; Jiang, P. Bioinspired Assembly of Surface-Roughened Nanoplatelets. *J. Colloid Interface Sci.* **2010**, *344*, 272–278.
35. Meyers, M. A.; Lin, A. Y.-M.; Chen, P.-Y.; Muyco, J. Mechanical Strength of Abalone Nacre: Role of the Soft Organic Layer. *J. Mech. Behav. Biomed.* **2008**, *1*, 76–85.
36. Barthelat, F.; Espinosa, H. D. An Experimental Investigation of Deformation and Fracture of Nacre-Mother of Pearl. *Exp. Mech.* **2007**, *47*, 311–324.
37. Meyer, R. W.; Pruitt, L. A. The Effect of Cyclic True Strain on the Morphology, Structure, and Relaxation Behavior of Ultra High Molecular Weight Polyethylene. *Polymer* **2001**, *42*, 5293–5306.
38. Bai, S. L.; Wang, M. Plastic Damage Mechanisms of Polypropylene/Polyamide 6/Polyethelene Octene Elastomer Blends under Cyclic Tension. *Polymer* **2003**, *44*, 6537–6547.
39. Pruitt, L. A. Deformation, Yielding, Fracture and Fatigue Behavior of Conventional and Highly Cross-Linked Ultra High Molecular Weight Polyethylene. *Biomaterials* **2005**, *26*, 905–915.